IJMMM International Journal of Minerals, Metallurgy and Materials 矿物冶金与材料学报（英文版）

Mechanisms and interactions in the reduction of Fe_2O_3 by H_2/CO mixed gas: Atomic insights from ReaxFF molecular dynamics simulations and experiments

Qiang Cheng, Alberto N. Conejo, Jianliang Zhang, Daniel Sopu, Yaozu Wang, and Zhengjian Liu

Cite this article as:
Qiang Cheng, Alberto N. Conejo, Jianliang Zhang, Daniel Sopu, Yaozu Wang, and Zhengjian Liu, Mechanisms and interactions in the reduction of Fe_2O_3 by H_2/CO mixed gas: Atomic insights from ReaxFF molecular dynamics simulations and experiments, *Int. J. Miner. Metall. Mater.*, 32(2025), No. 6, pp. 1372-1382. https://doi.org/10.1007/s12613-024-3061-y

---

INTERNATIONAL JOURNAL OF
Minerals, Metallurgy and Materials

Volume 32, Number 6, June 2025
Page 1372

Research Article https://doi.org/10.1007/s12613-024-3061-y

Mechanisms and interactions in the reduction of Fe_2O_3 by H_2/CO mixed gas: Atomic insights from ReaxFF molecular dynamics simulations and experiments

Qiang Cheng[1)], *Alberto N. Conejo*[1)], *Jianliang Zhang*[1)], *Daniel Sopu*[2)], *Yaozu Wang*[3)], *and Zhengjian Liu*[1),✉]

1) School of Metallurgical and Ecological Engineering, University of Science and Technology Beijing, Beijing 100083, China
2) Erich Schmid Institute of Materials Science, Austrian Academy of Sciences, Leoben 8700, Austria
3) Institute of Artificial Intelligence, University of Science and Technology Beijing, Beijing 100083, China
(Received: 19 September 2024; revised: 4 December 2024; accepted: 5 December 2024)

Abstract: The experiment explored the Fe_2O_3 reduction process with H_2/CO mixed gas and confirmed a promoting effect from CO when its volume proportion in mixed gas is 20% at 850°C. The ReaxFF molecular dynamics (MD) simulation method was used to observe the reduction process and provide an atomic-level explanation. The accuracy of the parameters used in the simulation was verified by the density functional theory (DFT) calculation. The simulation shows that the initial reduction rate of H_2 is much faster than that of CO (from 800 to 950°C). As the reduction proceeds, cementite, obtained after CO participates in the reduction at 850°C, will appear on the iron surface. Due to the active properties of C atoms in cementite, they are easy to further react with the O atoms in Fe_2O_3. The generation of internal CO may destroy the dense structure of the surface layer, thereby affecting the overall reduction swelling of Fe_2O_3. However, excess CO is detrimental to the reaction rate, mainly because of the poor thermodynamic conditions of CO in the temperature range and the molecular diffusion capacity is not as good as that of H_2. Furthermore, the surface structures obtained after H_2 and CO reduction have been compared, and it was found that the structure obtained by CO reduction has a larger surface area, thus promoting the subsequent reaction of H_2.

Keywords: hydrogen reduction; hydrogen/carbon monoxide mixture; ReaxFF molecular dynamics simulations; reduction swelling; atomic mechanisms

1. Introduction

In iron production, direct reduction refers to a process that does not involve melting the ore. Iron ore is reduced in its solid state, frequently utilizing reduction gases or coal as a reducing agent [1–5]. The resulting product is designated as direct reduced iron (DRI) or sponge iron, which can subsequently be employed in the steelmaking process [6–7]. Reduction gases typically contain H_2 and CO in direct reduction processes. Based on the requirement of low carbon environment, the development of hydrogen-based reduction technologies is a viable path [8–9]. Therefore, it is of research value to analyze the influence of temperature, gas composition, and other factors on the reduction process [10–11]. The effect of H_2/CO gas composition on the reduction of hematite was further investigated [12–13]. The selection of CO and H_2 as reducing agents is discussed, with CO identified as the more effective reducing agent at a lower temperature from a thermodynamic perspective while it will produce more CO_2 [14]. Phase transitions are defined as the changes in the physical and chemical states of iron ore that occur as a result of reduction, which is a crucial process for controlling the quality of DRI. The interplay between the aforementioned factors results in the formation of intricate microstructures, which are characterized by a diverse range of defects spanning multiple orders of magnitude in length. These include but are not limited to, vacancies, dislocations, internal interfaces, and free surfaces in the form of cracks and pores [15]. Among these, the formation of cementite has a more significant effect on the structure change during the reduction process. Zhang *et al.* [16] revealed that cementite may be generated in the middle and late stages of reduction due to the involvement of CO and the C/Fe mass ratio on the surface has a significant influence on the stickiness and also the fluidization behavior of DRI particles.

To better understand the transformation of Fe_2O_3 to Fe on an atomic scale and to summarize the laws involved, the density functional theory (DFT) approach is often used to study the system of reduction reactions [17–19]. DFT can provide detailed insights into the fundamental mechanisms and energetics involved in the reduction process, including the transition from Fe_2O_3 (hematite) to Fe_3O_4 (magnetite) and

✉ Corresponding author: Zhengjian Liu E-mail: liuzhengjian@ustb.edu.cn

ultimately to metallic iron (Fe). Wang and Li [20] addressed this challenge and puts forward a DFT-based microkinetic rate equation theory to calculate the heterogeneous kinetics of Fe_2O_3 reduction by CO in chemical looping. At the atom scale, the surface reaction mechanism of H_2 with Fe_2O_3 was investigated based on DFT calculations [21].

DFT is a highly efficient and widely applicable computational method that provides excellent accuracy for ground-state properties across a diverse range of systems. However, due to the limitation of computational ability, DFT is often applied to structures with small scales, generally within the nanometer scale. ReaxFF molecular dynamics (MD) method was born with great computational power and relative accuracy [22–24]. In contrast to conventional force fields, which are generally constrained to modelling fixed bond topologies, ReaxFF permits the dynamic formation and dissolution of chemical bonds during a simulation [25–26]. Van Duin's group [27] first applied the ReaxFF method to the Fe system and developed a set of Fe/H/C/O potentials. The accuracy of the existing ReaxFF Fe/C/O/H description is evaluated, thereby furnishing indispensable data regarding the specific areas that require further enhancement. Additionally, reaction processes involving iron-related compounds such as Fe_2S and iron oxides with gas-phase molecules have been investigated to develop more systems and create more possibilities. Shin *et al*. [28] developed a ReaxFF force field for Fe/Cr/O/S based on the oxidation of butane over a pyrite-covered Cr_2O_3 catalyst, which is parametrized against data from quantum mechanical (QM) calculations.

Numerous studies have examined gas composition, temperature, and pressure effects on direct reduction [29–31]. However, comprehensive analyses of reduction mechanisms at the atomic level across different reduction stages remain limited. In addition, it has been found experimentally that CO seems to have a facilitating effect on the reduction of H_2 under specific conditions. It has been reported that the group of 80vol%H_2–20vol%CO at 850°C could promote the overall reduction to a rate exceeding that of 100% H_2 [32]. This is an important topic that deserves specific investigation using computational simulations. DFT uses quantum mechanics to calculate the charge transfer between atoms, whereas MD study calculates the forces between atoms based on Newton's laws, often used in a much larger system [33–34]. Unlike other computational studies, this study is based on experimentally phenomena and employs simulations to explain the mechanisms and obtains more compatible results.

In this study, reduction experiments and ReaxFF MD simulations were combined to summarize the effect of H_2–CO mixed gas on the reduction pattern. The effect of different gas components on the reduction rate was analyzed. X-ray diffraction (XRD) and scanning electron microscopy–energy dispersive spectroscopy (SEM–EDS) tests were used to investigate the transformation patterns and structural characteristics of the phases during the reduction process. The accuracy of the parameters was verified by the DFT method prior to simulation. The relative energies of H_2 and CO as a function of bond length and the variation of Fe and Fe_2O_3 as a function of cell volume were tested to determine the applicability of the parameters. Different simulation structures were created to reflect the different gas–solid reactions at the beginning and middle stages of reduction process. Furthermore, the factors affecting the reduction swelling were analyzed in detail.

2. Experimental

2.1. Reduction experiments

Reduction method was used to analyze the effect of gas components on reduction rates. As shown in Fig. 1(a), the experiments are divided into four steps. (1) The amount of 3.00 g Fe_2O_3 powder with a purity of more than 99.9% was pressed using a cylindrical mold. (2) To increase its strength of the obtained cylindrical sample, it was calcined at 1000°C for 3 h under the protection of pure argon. (3) The obtained high-strength sample was placed in a tube furnace for reduction testing. The used equipment is shown in Fig. 1(b). The

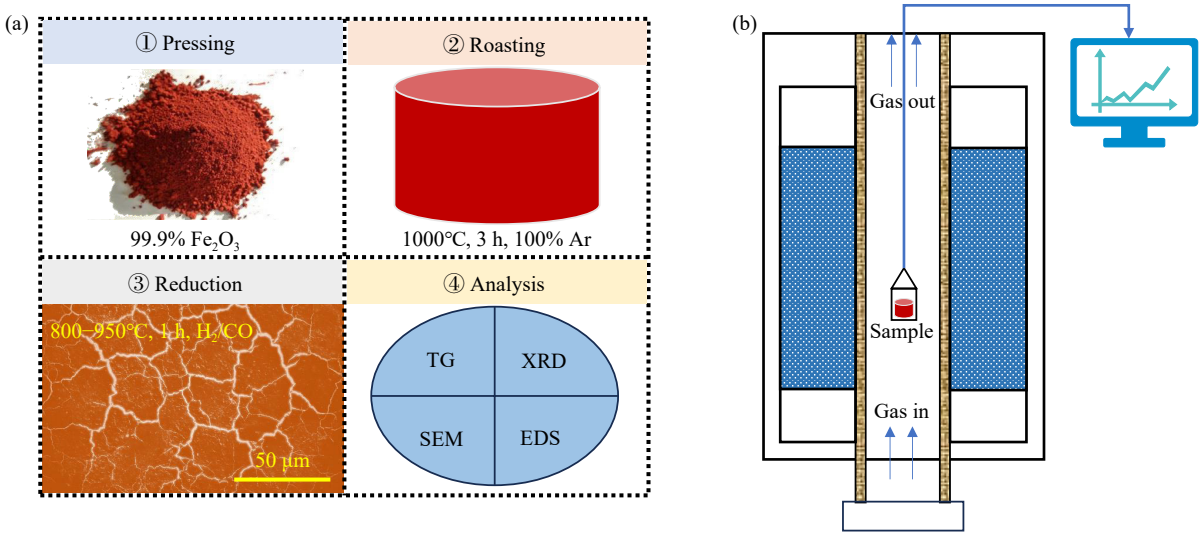

Fig. 1. (a) Experimental procedure comprising pressing, roasting, reduction, and analysis; (b) equipment used in the roasting and reduction experiments. TG—Thermogravimetric.

protective gas and the reducing gas were input from the bottom and flowed out from the top. The sample was placed in the middle hanging basket and connected to a balance with a computer for weight detection. The reduction rate can be reflected by the change in the mass of sample. The main principle is that Fe_2O_3 undergoes a step-by-step reduction reaction to generate metallic Fe after contacting CO and H_2. (4) Reduced samples were finally analyzed by XRD and SEM–EDS. The type of equipment for XRD analysis is X'Pert PRO MPD with a scanning speed of 2°/min. The type of SEM–EDS equipment is FEI Quanta and has a resolution of 3 nm under vacuum condition.

The specific details of the reduction experiment are listed in Table 1. The components of 5 different mixed gases were compared. The effects of reduction temperature on the reduction rate were investigated, and the temperature of 800, 850, 900, and 950°C were set respectively. The reference principle for temperature setting is the reduction processes of Midrex and HYL [35–37]. This temperature range is the advantage zone of H_2 reduction, aiming to explore the influence of CO addition on H_2 reduction.

Table 1. Conditions of a series of reduction experiments

Series	Mixed gas composition / vol%		Temperature / °C
	H_2	CO	
1 ($100H_2$)	100	0	800, 850, 900, or 950
2 ($80H_2$/20CO)	80	20	800, 850, 900, or 950
3 ($50H_2$/50CO)	50	50	800, 850, 900, or 950
4 ($20H_2$/80CO)	20	80	800, 850, 900, or 950
5 (100CO)	0	100	800, 850, 900, or 950

2.2. ReaxFF methods

ReaxFF MD simulation is a computational method based on classical MD and incorporated exchange for chemical reaction systems calculation. Therefore, the breakage and synthesis of chemical bonds is an important characterization. This method uses DFT fitting parameters to express the interaction between atoms through specific formulas. ReaxFF has been applied to a diverse range of chemical systems, including hydrocarbons, ceramics, metals, polymers, and biomolecules. Its ability to handle large systems with thousands or millions of atoms makes it particularly useful for studying many processes. Since the research system involves the reaction between gas phase and solid phase, this method is applicable. As shown in Eq. (1), the energy in the system includes bond energy (E_{bond}), over- and under-coordinated energy correction (E_{over} and E_{under}), lone pair electron energy (E_{lp}), bond angle energy (E_{val}), dihedral energy (E_{tor}), van der Waals force ($E_{vdWaals}$), and Coulomb force ($E_{Coulomb}$).

$$E_{system} = E_{bond} + E_{over} + E_{under} + E_{lp} + E_{val} + E_{tor} + E_{vdWaals} + E_{Coulomb} \quad (1)$$

As shown in Fig. 2, the two main systems are calculated, namely the reaction processes of Fe_2O_3 and metal Fe substrates with gas molecules. The first reaction system expresses the initial reaction between reducing gas and iron oxide. The total number of gas phase molecules is set to 200, and the Fe_2O_3 substrate is set to 40 Å × 40 Å with a thickness of 12 Å. Considering the changes in the surface in the middle and late stages of the reaction, the second reaction system covers 10 Å of iron carbide on the Fe_2O_3 substrate. The reaction is set to NVT system, the reaction time is set to 200 ps, and the step size is as 0.25 fs. The *XY* directions are set as a periodic boundary, and the both sides in *Z* direction are set as the unreacted region.

2.3. Parameters validation

To demonstrate the advantages of the ReaxFF method, which has a high computational efficiency and capacity for larger atomic systems, we verify the accuracy of parameters through comparison with the DFT (GGA-PBE) results [38–39]. The parameters initially developed by van Duin's group and subsequently optimized. To verify their applicability in this research system, relative energy tests were performed on H_2, CO, Fe, and Fe_2O_3, as depicted in Fig. 3. Relative energy is a fundamental concept in understanding and predicting the behavior of physical and chemical systems, particularly in computational modeling and theoretical studies. Generally speaking, a molecule has a fixed length of chemical bonds at their lowest energy state, which is called a steady state. Therefore, we first compared the relative energy changes of H_2 and CO obtained by DFT and ReaxFF meth-

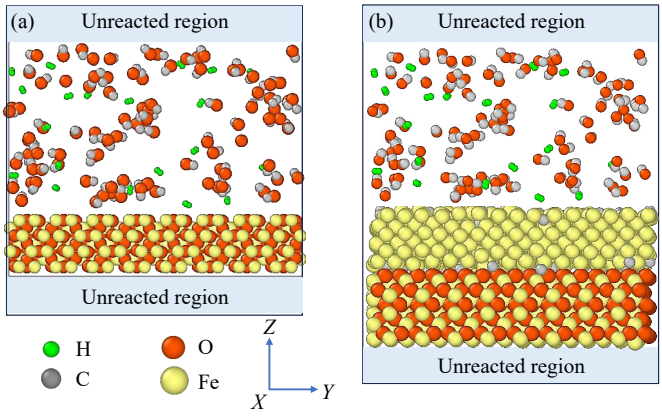

Fig. 2. Reaction systems: (a) initial system; (b) mid stage system.

ods. The results show that the system reaches steady state at a bond length of H_2 bond length of 0.74 Å, which is completely consistent with the experimental results. Similarly, CO exhibits its lowest energy at 1.13 Å, which is also very close to the experimental data. Steady-state cell volume is often studied in DFT and MD simulations to define the perfect size of the given structure. The most stable volume of Fe (body-centered cubic, i.e., bcc) unit cell calculated by ReaxFF is 23.22 $Å^3$, which has a 1.3% decrease compared to that by DFT, almost showing a good performance. For the Fe_2O_3 unit cell, the most stable sizes measured by two methods differ by about 3.5%, which is mainly due to the complexity of the oxide system compared to pure metals. This deviation remains within a reasonable range and there is a possibility of continuous optimization in the future. Therefore, all parameters used in this study are scientific and reproducible. The outcomings have been analyzed using Ovito and visual molecular dynamics (VMD) [40–41].

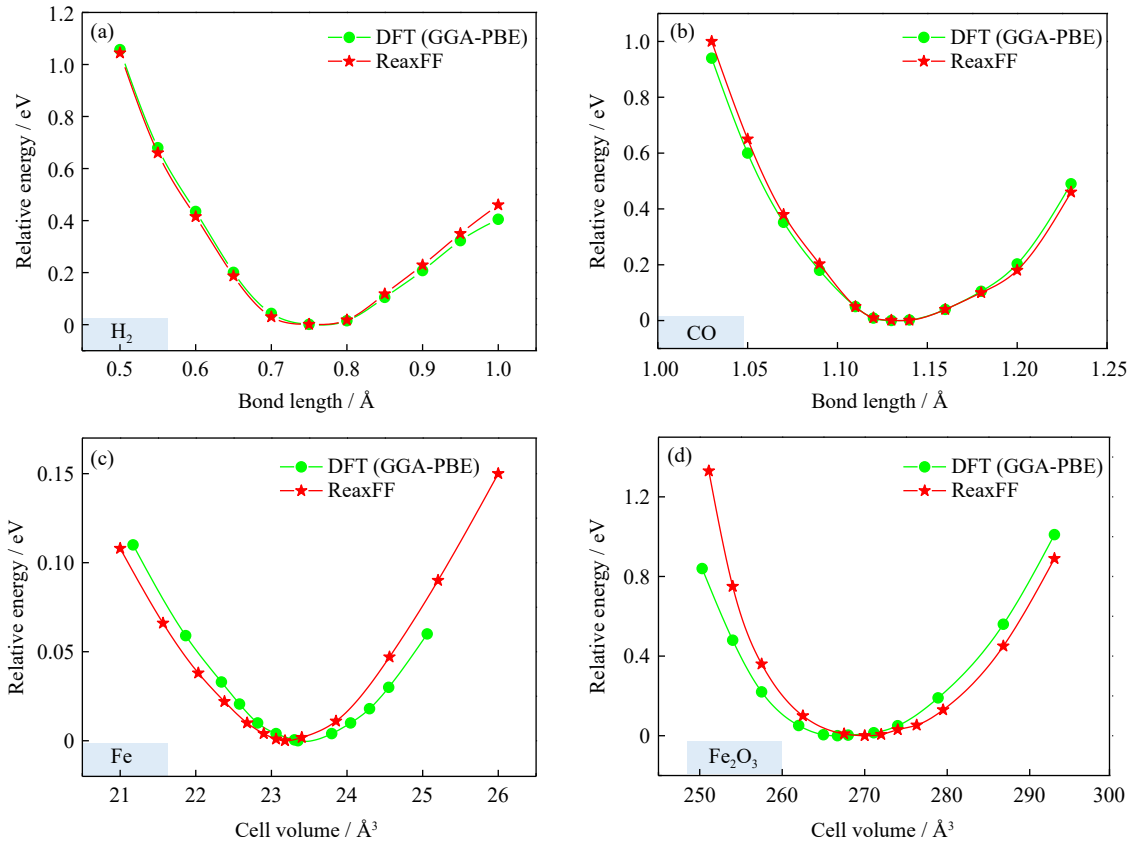

Fig. 3. Validation of simulation methods for all systems by checking the relative energy of (a) H_2 bond length, (b) CO bond length, (c) Fe cell volume, and (d) Fe_2O_3 cell volume.

3. Results and discussion

3.1. Fe_2O_3 reduction using H_2 and CO

The Fe_2O_3 reduction process involves two primary reactions. In Eq. (2), CO reduces Fe_2O_3 to iron, producing carbon dioxide as a by-product. In Eq. (3), H_2 acts as the reducing agent, reducing Fe_2O_3 to iron, generating water vapor as a by-product. Fig. 4 shows the reduction curves under different gas components from 800 to 950°C, and two main obvious phenomena can be found. First, the higher the temperature, the faster the reduction rate. At 950°C with pure H_2, the reduction endpoint is basically reached within 14 min whereas at 800°C with pure H_2, the reaction remains incomplete even after 30 min. Second, H_2 is more reactive than CO, particularly at higher temperatures, which can lead to faster reduction rates. These phenomena can be explained by that hydrogen is a lighter and more reactive molecule than CO, which can penetrate the iron ore particles more easily and promote faster reduction rates, especially beneficial at higher temperatures, where the reduction rate of H_2 exceeds that of CO. However, it is worth noting that at 850°C, the sample has the fastest reduction rate under the particular composition (80vol%H_2–20vol%CO), which indicates that the addition of a small amount of CO can effectively promote the overall reduction. Initially, this result was suspected to be an accidental error in the test, but the repeated experiment has once again confirmed this phenomenon. The reason for this result may be the phase transition during the reduction process affecting the kinetic conditions of the chemical reaction.

$$Fe_2O_3 + 3CO = 2Fe + 3CO_2 \quad (2)$$

$$Fe_2O_3 + 3H_2 = 2Fe + 3H_2O \quad (3)$$

To further explore how the addition of a small amount of CO promotes reduction at 850°C, we compared the reduction process of Sample 1 and Sample 2, which represents the samples obtained at 850°C with the gas conditions of 100% H_2 and 80vol%H_2–20vol%CO, respectively. For a Fe_2O_3

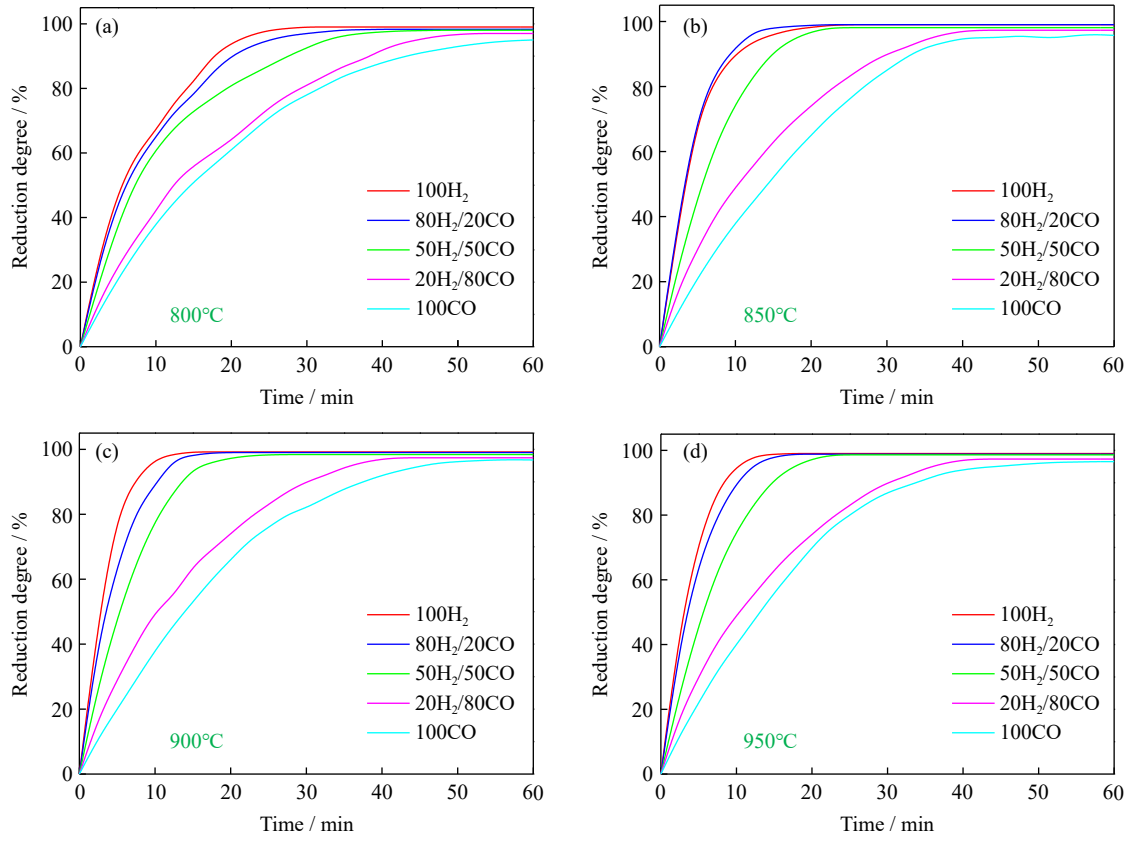

Fig. 4. Changes in reduction degree under different gas compositions at (a) 800°C, (b) 850°C, (c) 900°C, and (d) 950°C.

particle, the reduction is carried out from the outer layer to the inside. The reduction of the outer layer is a surface reaction where the reducing gas (CO or H_2) reacts with oxygen atoms on the surface of the metal oxide, forming gaseous by-products like CO_2 or H_2O and leaving behind a partially reduced metal oxide. The outer layer always forms metallic iron first. To understand the process of subsequent reduction of the gas and the internal iron oxide in the middle stage of reduction, SEM and EDS were used to analyze Sample 1 and Sample 2 after 10 min of reduction, as shown in Fig. 5(a) and (b). The interior of the grain can still maintain a relatively dense state, while more cracks and pores appear in the outer layer of the grain. The outer layer of the particle in Sample 1 after 10 min reduction is almost pure metallic iron (refer to

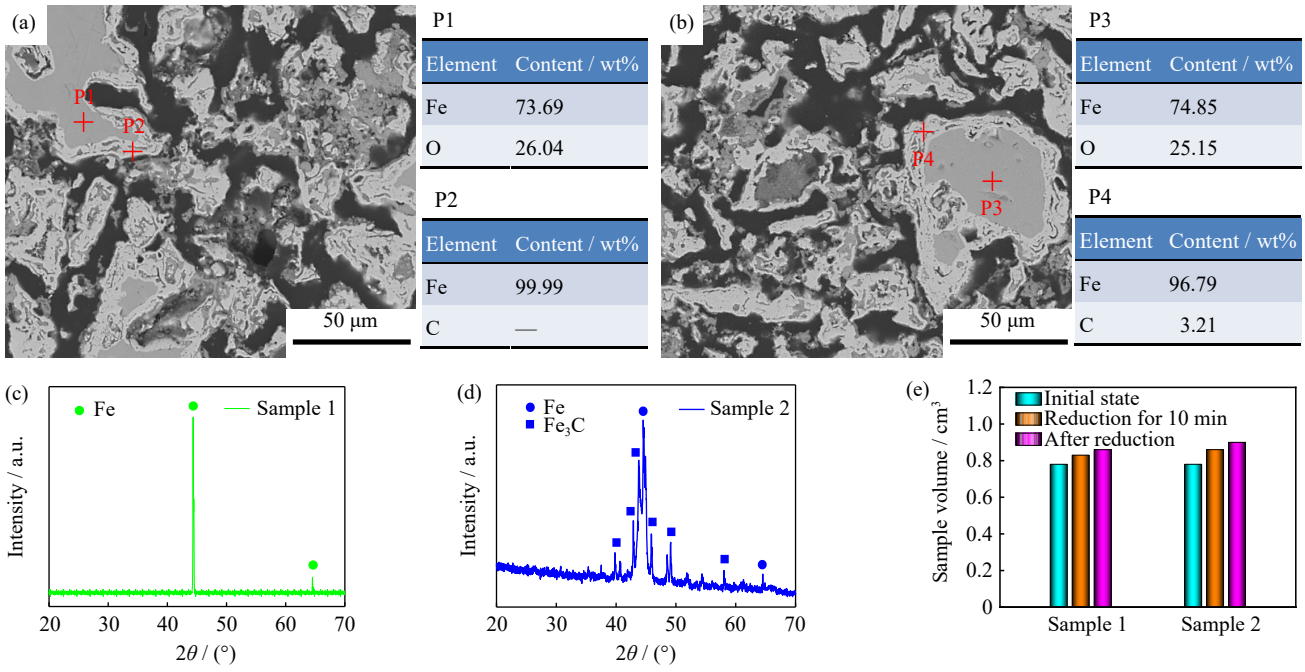

Fig. 5. SEM and EDS analysis of (a) Sample 1 after reduction for 10 min and (b) Sample 2 after reduction for 10 min; XRD analysis of (c) Sample 1 after reduction and (d) Sample 2 after reduction; (e) volume change of Sample 1 and Sample 2 in different stages.

P2), while the darker area inside is still in the state of iron oxide (refer to P1), which indicates that the reduction is not yet sufficient. In contrast, the elemental analysis of the outer layer in Sample 2 after 10 min reduction shows a certain amount of C, which indicates that iron carbide may have formed in this area.

After complete reduction, the sample was cooled to room temperature under Ar protection and preserved. XRD detection was used to specifically explore the final phase composition of the samples. Fig. 5(c) and (d) reveals that the final phase of Sample 1 is pure metallic iron, and no other peaks are found in the curve. Sample 2 mainly includes two phases, metallic iron and Fe_3C. By analyzing the variation in the mass of the sample (from 2.10 to 2.15 g), it is possible to accurately calculate the percentage of Fe_3C in the sample as 35.7wt%. Therefore, at a specific temperature (850°C), the addition of CO may cause the formation of iron carbide. In addition, the volume change of the samples was statistically analyzed, and it was found that the volume change after the addition of CO was more obvious, expanding by about 15.4%. The series of phenomena show that the addition of CO causes the appearance of iron carbide in out layer in the middle stage of reduction, which makes it easier for volume expansion to occur there. The loose structure caused by volume expansion is more conducive to gas diffusion and promotes deep reduction [42–43]. It is shown that the reduction swelling of the pellets further enlarges with the increasing CO content and the overall structure becomes loose. However, at the same time, a large amount of CO occupies the reaction sites on the surface of iron oxides. Moreover, the reaction rate of CO is lower than that of H_2. Therefore, the overall reduction rate decreases with the increasing concentration of CO.

The data of different gas flow rates at 850°C are recorded in Table 2. The gas utilization rate can be calculated by detecting the top gas components at different times. I_0 is defined as the initial utilization rate at the beginning of reduction, and I_R is defined as the average utilization rate during the entire reduction process. The results show that as the reduction progresses, the gas utilization rate continues decreasing, and the initial gas utilization rate is always the highest. The initial and average gas utilization rates have been calculated in Table 2. The reduction can be divided into three stages. At the early stage, all CO is used to reduce the O atoms in the iron oxide. In the middle stage of reduction, metallic iron appears in the outer layer of the pellet, at which time most of the CO is still consumed by reduction, and a small amount of CO reacts with the metallic iron to form Fe_3C. In the late stage, the O atoms in the samples have already been consumed, and all the CO is used to combine with the iron to form cementite.

Table 2. Utilization rate of H_2 and CO including initial utilization rate and average utilization rate at 850°C

No.	H_2 flow rate / (L·min^{-1})	CO flow rate / (L·min^{-1})	I_0 of H_2 / %	I_0 of CO / %	I_R of H_2 / %	I_R of CO / %
1	2.0	0	48.1	—	14.2	—
2	1.6	0.4	50.2	51.9	14.8	15.8
3	1.0	1.0	51.8	50.6	15.6	15.3
4	0.4	1.6	53.6	49.3	16.1	14.7
5	0	2.0	—	47.6	—	13.9

3.2. ReaxFF MD simulations on H_2/CO with Fe_2O_3

In this part of the study, to be consistent with the reduction experiment, the temperature of 850°C has been chosen as the characteristic temperature for exploration. First, the reduction process of Fe_2O_3 under H_2 and CO conditions was compared. Fig. 6(a) depicts the system composition after H_2 reduction. It can be found that the structure of Fe_2O_3 has changed significantly, and a large number of water vapor molecules are attached to the surface. Another part of the water vapor migrates to the gas phase. Fig. 6(b) details the formation process of H_2O. First, hydrogen molecules are adsorbed on the surface by intermolecular forces, and then H_2 dissociates at high temperature to obtain two separate H atoms. H atoms and O atoms can easily exchange charges, form chemical bonds, and generate H_2O. The obtained water molecules are active at high temperatures and have a certain probability of migrating to the gas phase. In the molecular dynamics research system, the rate of various processes is often reflected by the change of the products. Therefore, the change in the number of H_2O molecules and H_2 molecules can intuitively reflect the reduction rate. Fig. 6(c) describes that hydrogen is continuously reduced at a fast rate and is completely consumed within about 55 ps, transforming into 100% water molecules. Fig. 6(d)–(f) examines Fe_2O_3 reduction process by CO through similar analysis. The results show that the reduction of CO can also be divided into the following stages. First, CO is adsorbed, and the C atoms in CO transfer charge with the O atoms on the surface of Fe_2O_3 to form chemical bonds. After bonding, C–O continuously adjusts the length and angle until the three atoms are adjusted to a straight line, generating CO_2 molecules and returning to the gas phase. Unlike H_2, the overall reduction efficiency of CO is slow and has a reduction limit, hence it cannot be completely converted into CO_2. At 200 ps, 39vol% CO_2 has been produced. Finally, reduction processes of three mixed gases are further compared. The results shown in Fig. 6(g)–(i) reveal that the higher the CO content, the lower the overall reduction rate. However, the addition of 20vol% CO significantly increases the H_2 consumption rate. H_2 is completely consumed in just 40 ps with addition of 20vol% CO, which is faster than the 55 ps required without CO addition. This is consistent with the results obtained from the reduction experiments. When the volume content of CO reaches 50%, the H_2 consumption rate decreases significantly, mainly because a

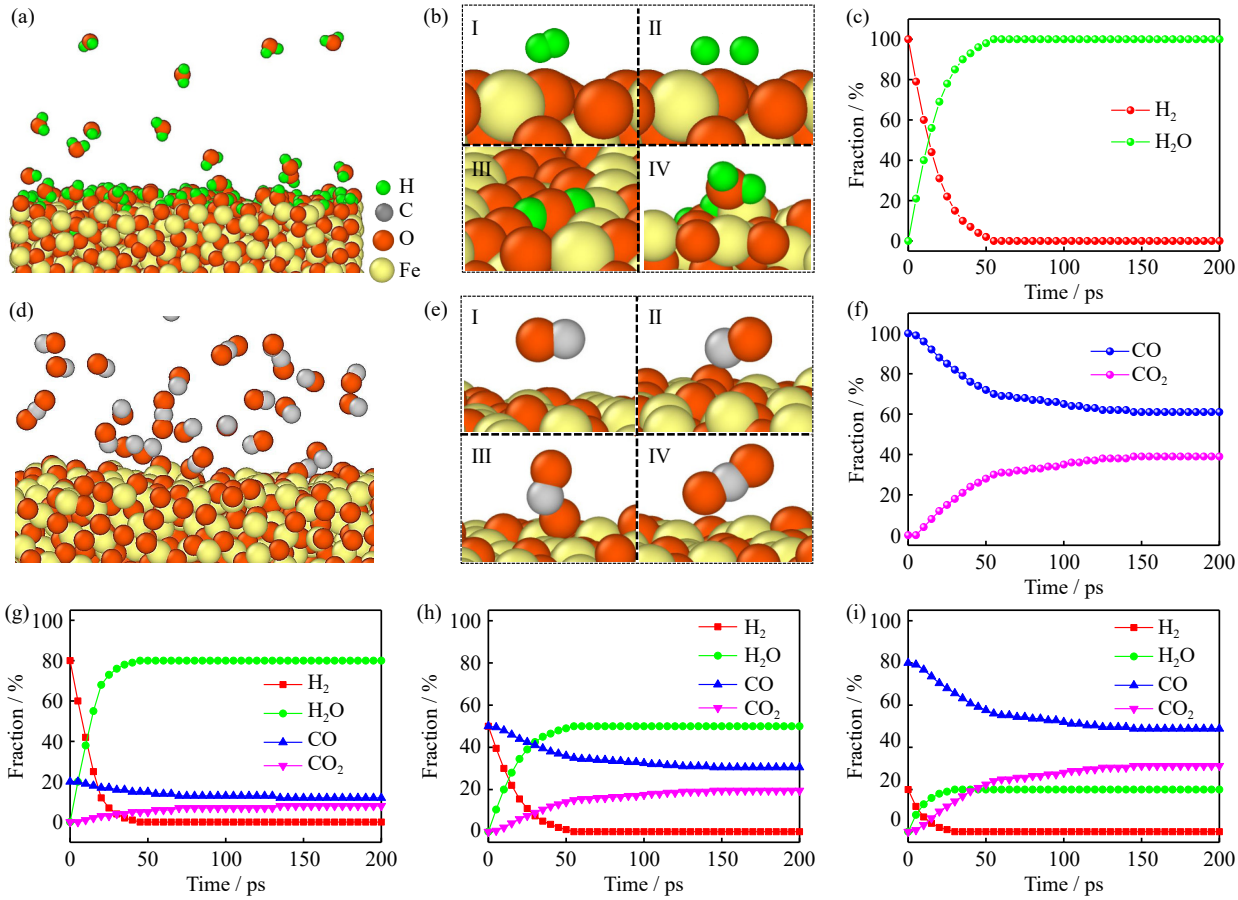

Fig. 6. (a) Snapshots of Fe_2O_3–H_2 after 200 ps, (b) the formation process of H_2O, (c) changes in gas molecule content of 100% H_2, (d) snapshots of Fe_2O_3–CO after 200 ps, (e) the formation process of CO, (f) changes in gas molecule content of 100% CO, (g) changes in gas molecule content of 80vol%H_2–vol20%CO, (h) changes in gas molecule content of 50vol%H_2–50vol%CO, and (i) changes in gas molecule content of 20vol%H_2–80vol%CO.

large number of CO molecules in the gas phase will occupy the effective adsorption sites on the Fe_2O_3 surface. These simulation results only display the interaction between the gas and Fe_2O_3 surface in the initial stage of the reduction. To more clearly understand the formation of metallic iron in subsequent reduction process, the structure after 200 ps of reduction has been re-input each time, and the reducing gas will be inserted for simulation, and this cycle repeats until the O atoms in Fe_2O_3 are completely consumed.

After multiple cycles of reduction, the reduced structure is obtained. This section mainly compares the effects of H_2 and CO on the products obtained after reduction. The primary advantage of using hydrogen as a reducing agent is the significant reduction in carbon emissions. Instead of producing CO_2 as by-product in traditional carbon-based processes, the byproduct of hydrogen reduction is water vapor (H_2O), making it a much cleaner process. At 850°C, metallic iron is in the alpha iron (ferrite) phase with a bcc structure. Although iron has lost its magnetism at this point, its crystal structure has not yet transformed into the face-centered cubic structure at higher temperatures. Iron at this temperature is still a solid metal with good ductility and relatively low strength. Fig. 7(a) shows the crystal structure after complete H_2 reduction. The structure is metallic iron, and no other elements are found. The radial distribution function (RDF) method was used to explore the specific arrangement of atoms. Metallic iron is with an obvious crystal structure with a clear peak at 2.48 Å between Fe atoms, which is consistent with the characteristic bcc Fe structure (Fig. 7(b)).

For CO reduction process, carburization reaction will occur in the middle and late stages of reduction, mainly because CO will decompose under specific conditions. As CO continuously reduces iron oxides, all O atoms from the Fe_2O_3 surface react. The newly generated metallic iron has a certain catalytic effect on the decomposition of CO. Due to the strong effect of Fe–C, CO is first adsorbed on the iron atom. When another CO migrates nearby, the C–O bond is activated and then broken, generating CO_2 while leaving a C atom sandwiched in the iron lattice. C atoms can continuously migrate in iron and form cementite at a certain temperature. Fig. 7(c) describes the final structure after CO reduction. It can be seen that the metallic iron contains a large number of C atoms, which are widely distributed throughout the structure. Fe_3C structure exhibits strong interaction between iron atom and carbon atom, forming Fe–C bonds that combine the properties of metallic and covalent bonds. The bond length between Fe and C ranges from about 1.98 to 2.03 Å, depending on the position of the atoms in the unit cell. The RDF analysis in Fig. 7(d) reveals that part of the structure shows the bcc metallic iron (peak position is 2.48 Å), and another

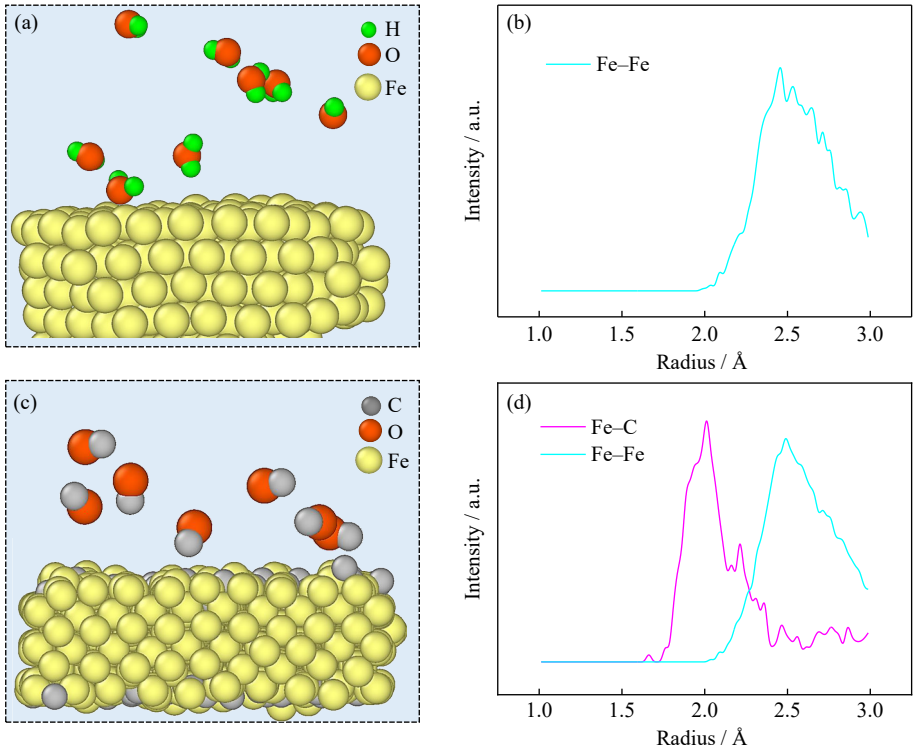

Fig. 7. (a) Structure after H_2 reduction, (b) RDF of the structure obtained by H_2 reduction, (c) structure after CO reduction, and (d) RDF of the structure obtained by CO reduction.

part of the structure shows the Fe–C bonds (peak position is 2.00 Å), consistent with the characteristics of cementite structure.

3.3. Expansion effect caused by CO reduction

Through the previous stage of research, it has been proved that when CO participates in the reduction, cementite will be preferentially obtained on the surface in the middle and late stages. Cementite (Fe_3C), is a metastable phase in the iron–carbon system. It can decompose into iron and carbon under certain conditions. This decomposition is a key part of processes like the tempering of steel and the production of malleable iron. Fe_3C is stable at lower temperatures but will decompose at higher temperatures. The decomposition is influenced by both the temperature and the presence of other phases. The obtained cementite structure is covered on the upper layer of Fe_2O_3 and performs as a channel for the continuous development of reduction from outer layer to inner layer in the middle stage. As shown in Fig. 8(a), when CO transfers into CO_2, some of the C atoms will form Fe_3C. In addition, the surface structure of the substrate has changed significantly and is no longer a regular iron crystal. As shown in Fig. 8(b) and (c), the structure before and after the reaction has been sliced along *Z* direction, and the specific transformation path of the C atoms has also been discovered. Before the reaction, a part of C atoms exists in the cementite, and its properties are relatively active, so it is easy to migrate in the lattice. It is found that a part of CO is still retained in the interface between Fe_3C and Fe_2O_3 after the deep reduction. These internal CO have a tendency to migrate to the surface, which is mainly because CO is large in volume and difficult to effectively exist in metal or metal oxide structures. The large internal pressure forces CO to migrate to the surface and return to the gas phase. In addition, obvious cracks appear on the surface structure, suggesting that the process of CO escaping to the surface is likely to cause the structure to expand and form the cracks.

The migration of O atoms is also an important phenomenon in the middle stage of reduction. Fig. 8(d) briefly describes the average diffusion depth of C atoms. Due to the concentration difference caused by the high C content on surface will migrate to metallic iron at a certain temperature. The primary driving force for concentration diffusion is the concentration gradient. Atoms move to minimize this gradient, leading to a more uniform distribution of particular elements over time. At a high temperature, due to the higher diffusion coefficient of C, they will diffuse into the iron lattice at a faster rate and reach a greater diffusion depth. At 950°C, the maximum diffusion depth reaches 2.935 Å. However, a high temperature will accelerate the decomposition of cementite. We keep the saturated cementite at constant temperature for 200 ps, and the results are shown in Fig. 8(e), which indicates that cementite may be more stable at low temperatures. The number of internal CO at different temperatures is statistically shown in Fig. 8(f). The reaction rate between C in Fe_3C and Fe_2O_3 is intensive at a high temperature and more CO can be generated. At 850°C, the presence of cementite gives a channel for the diffusion of C and O.

The iron slab obtained through pre-reduction by H_2 and CO exhibit different phase compositions and overall structural states. By comparing the structures of the substrates in Fig. 9(a) and (b), it can be clearly seen that there are obvious

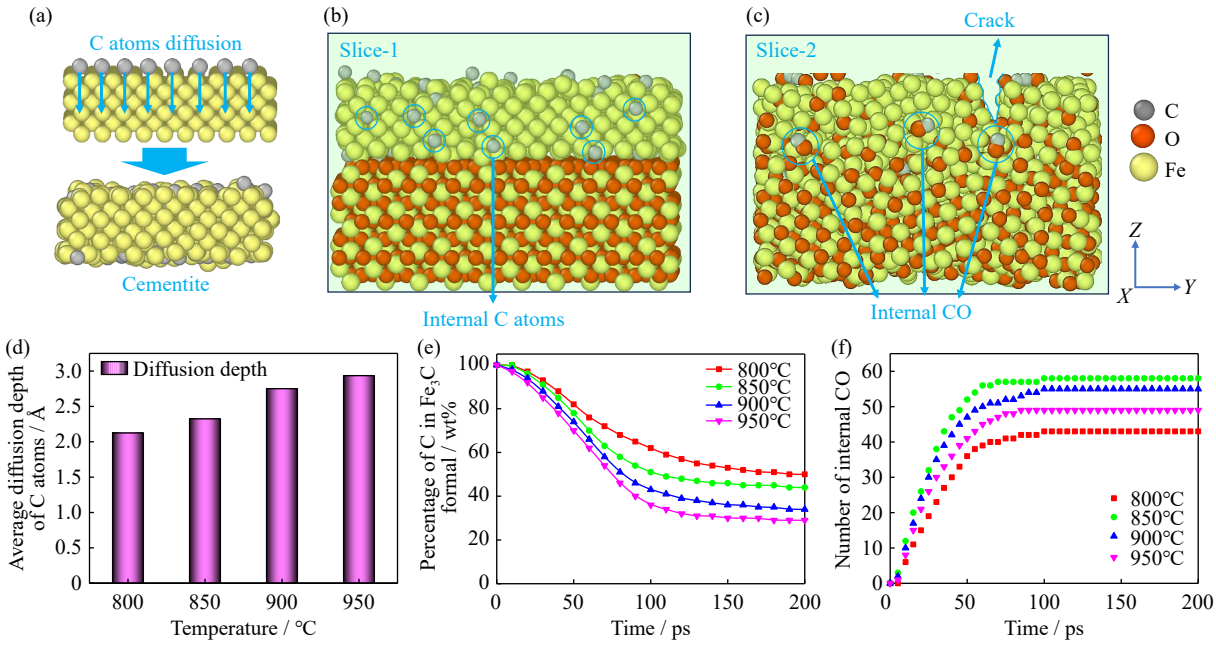

Fig. 8. Cementite formation and decomposition when CO participates in the reduction: (a) diffusion of C and formation of cementite; (b) snapshot of the initial structure by slice; (c) snapshot of the final structure by slice. (d) Average diffusion depth of C atoms, (e) decomposition curve of cementite, and (f) number of internal CO at different temperatures.

cracks in the substrate obtained by 80vol%H_2–20vol%CO pre-reduction. This result is consistent with the reduction experiment (the structure obtained by CO contained reduction has a higher reduction swelling index). The surface area caused by cracks, often referred to as the 'fracture surface area', which is the total area of the new surfaces generated when a material undergoes cracking or fracturing. Generally speaking, a structure with cracks trends to have a higher surface area. The specific details are recorded in Fig. 9(c), and it can be found that the structure obtained by CO contained pre-reduction does have a higher surface area. In addition, under higher temperature conditions, a relatively higher surface area can be obtained. This is because the substrate obtained by 80vol%H_2–20vol%CO pre-reduction contains more C atoms, and a higher temperature can promote the formation of CO at a faster rate. The concentrated CO is removed to the

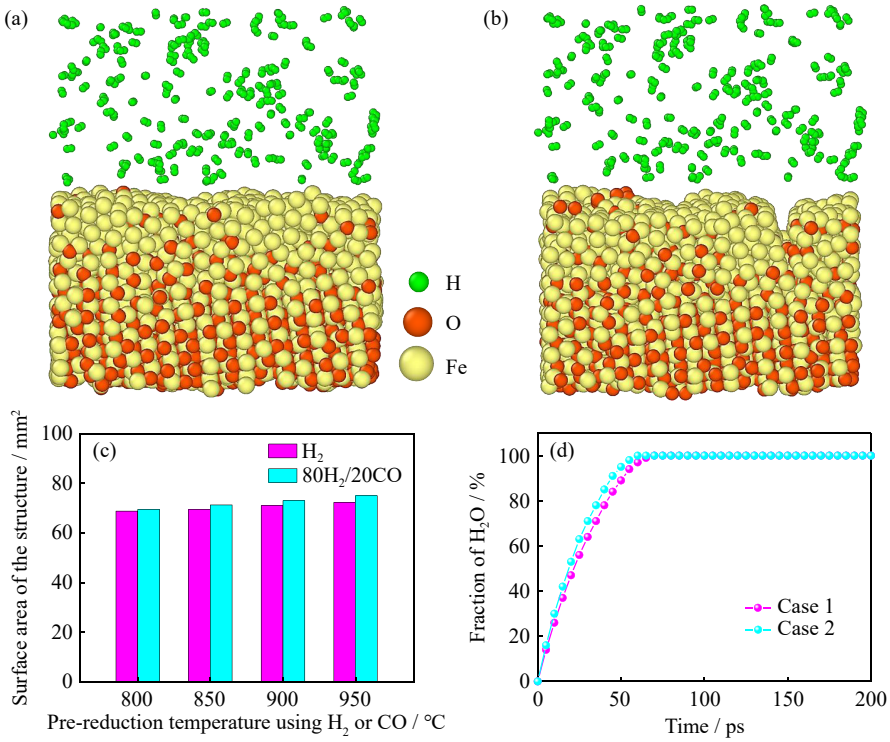

Fig. 9. Deep reduction of H_2 with the slab pre-reduced by (a) pure H_2 and (b) 80vol%H_2–20vol%CO; (c) surface area of the structure pre-reduced by pure H_2 and 80vol%H_2–20vol%CO; (d) synthesis rate curve of H_2O at 850°C on different substrates.

surface, which is more likely to cause cracks. Finally, H_2 molecules are inserted on the obtained substrate to explore the effect of different substrates on the deep reduction of H_2. Fig. 9(d) describes the reduction process of two different substrates. Case 1 represents the substrate obtained by H_2 pre-reduction, and case 2 is that obtained by 80vol%H_2–20vol%CO pre-reduction. The results show that case 2 has a higher reduction rate, which indicates that a higher surface area is conducive to increase the reaction frequency between H_2 and Fe_2O_3. Due to its small size and strong diffusion ability, H_2 can easily enter the structure through cracks and other loose locations, and further combine with O in the lattice to generate H_2O. The above simulations can explain that adding a certain amount of CO is beneficial to the formation rate of H_2O. Therefore, the 80vol%H_2–20vol%CO experimental group can obtain a faster reduction curve.

4. Conclusions

This investigation combines the experiments and computational simulations to present the following findings.

(1) A maximum reduction rate of 80vol%H_2–20vol%CO at 850°C was found, with the main difference being in the middle and late stages of reduction. The phenomenon is attributed to the generation of a small amount of cementite, which provides a good channel for the diffusion of C atoms, which in turn synthesizes internal CO. Therefore, a tendency for the enhancement of hydrogen utilization as the CO content increases.

(2) DFT calculations verify the accuracy and applicability of the parameters. The ReaxFF MD simulation results showed that H_2 has a high reduction rate and can completely consume H_2 before 55 ps. The iron layer obtained by H_2 reduction is a pure bcc structure (peak position of 2.48 Å), while that obtained by CO involved reduction contains a mixture of metallic iron and cementite (peak position of 2.00 Å).

(3) After the formation of cementite on the surface, a large amount of internal CO is easily generated at the interface of Fe_3C and Fe_2O_3 because of the C diffusion. The process of CO removal from the interface may cause cracks in the surface structure and increase the surface area which is conducive to increase the reaction frequency between H_2 and Fe_2O_3. The swelling ratio of the sample after adding 20vol% CO is higher than that obtained by pure H_2. These simulation results provide an atomic explanation for the experimental phenomenon. At the same time, it gives a relatively novel research idea for gas–solid reactions.

Acknowledgements

The authors acknowledge the financial support from the National Natural Science Foundation of China (Nos. 52204335 and 52374319), the National Nature Science Foundation of China (No. 52174291), and the Central Universities Foundation of China (No. 06500170).

Conflict of Interest

Alberto N. Conejo and Jianliang Zhang are the editorial board members for this journal and were not involved in the editorial review or the decision to publish this article. The authors declare that there is no conflict of interest.

References

[1] T. Battle, U. Srivastava, J. Kopfle, R. Hunter, and J. McClelland, The direct reduction of iron, [in] S. Seetharaman, R. Guthrie, A. McLean, S. Seetharaman, and H.Y. Sohn, *Treatise on Process Metallurgy*, 2nd ed., Elsevier, Amsterdam, 2024, p. 89.

[2] T. Harada and H. Tanaka, Future steelmaking model by direct reduction technologies, *ISIJ Int.*, 51(2011), No. 8, p. 1301.

[3] J. Wang, W. Wang, X.H. Chen, J.F. Bao, Q.Y. Hao, H. Zheng, and R.S. Xu, Role of iron ore in enhancing gasification of iron coke: Structural evolution, influence mechanism and kinetic analysis, *Int. J. Miner. Metall. Mater.*, 32(2025), No. 1, p. 58.

[4] H. Zhang, T.X. Wang, G.Y. Zhang, *et al*., Clean production of Fe-based amorphous soft magnetic alloys via smelting reduction of high-phosphorus iron ore and apatite, *Int. J. Miner. Metall. Mater.*, 30(2023), No. 12, p. 2356.

[5] J.G. Feng, J. Tang, Z.C. Zhao, *et al*., Effect of titanium on the sticking of pellets based on hydrogen metallurgy shaft furnace: Behavior analysis and mechanism evolution, *Int. J. Miner. Metall. Mater.*, 31(2024), No. 2, p. 282.

[6] B. Anameric and S. Komar Kawatra, Properties and features of direct reduced iron, *Miner. Process. Extr. Metall. Rev.*, 28(2007), No. 1, p. 59.

[7] S. Li, H.L. Zhang, J.P. Nie, R. Dewil, J. Baeyens, and Y.M. Deng, The direct reduction of iron ore with hydrogen, *Sustainability*, 13(2021), No. 16, art. No. 8866.

[8] A. Heidari, N. Niknahad, M. Iljana, and T. Fabritius, A review on the kinetics of iron ore reduction by hydrogen, *Materials*, 14(2021), No. 24, art. No. 7540.

[9] D. Spreitzer and J. Schenk, Reduction of iron oxides with hydrogen—A review, *Steel Res. Int.*, 90(2019), No. 10, art. No. 1900108.

[10] L.Y. Yi, Z.C. Huang, H. Peng, and T. Jiang, Action rules of H_2 and CO in gas-based direct reduction of iron ore pellets, *J. Cent. South Univ.*, 19(2012), No. 8, p. 2291.

[11] K. Rechberger, A. Spanlang, A.S. Conde, H. Wolfmeir, and C. Harris, Green hydrogen-based direct reduction for low-carbon steelmaking, *Steel Res. Int.*, 91(2020), No. 11, art. No. 2000110.

[12] C. Scharm, F. Küster, M. Laabs, *et al*., Direct reduction of iron ore pellets by H_2 and CO: *In situ* investigation of the structural transformation and reduction progression caused by atmosphere and temperature, *Miner. Eng.*, 180(2022), art. No. 107459.

[13] J.L. Yang, L.H. Li, Z.K. Liang, *et al*., Direct reduction of iron ore pellets by H_2–CO mixture: An *in situ* investigation of the evolution and dynamics of swelling, *Mater. Today Commun.*, 36(2023), art. No. 106940.

[14] B. Sadeghi, M. Najafizadeh, P. Cavaliere, A. Shabani, and M. Aminaei, Effect of composition and processing conditions on the direct reduction of iron oxide pellets, *Powder Technol.*, 444(2024), art. No. 120061.

[15] Y. Ma, I.R. Souza Filho, Y. Bai, *et al*., Hierarchical nature of hydrogen-based direct reduction of iron oxides, *Scripta Mater.*, 213(2022), art. No. 114571.

[16] T. Zhang, C. Lei, and Q.S. Zhu, Reduction of fine iron ore *via* a two-step fluidized bed direct reduction process, *Powder Technol.*, 254(2014), p. 1.

[17] W.H. Zhu, J. Winterstein, I. Maimon, *et al*., Atomic structural evolution during the reduction of α-Fe_2O_3 nanowires, *J. Phys.*

Chem. C, 120(2016), No. 27, p. 14854.
[18] C.F. Lin, W. Qin, and C.Q. Dong, H_2S adsorption and decomposition on the gradually reduced α-Fe_2O_3(001) surface: A DFT study, *Appl. Surf. Sci.*, 387(2016), p. 720.
[19] X.C. Liu, J. Tang, M.S. Chu, *et al*., Density functional theory study on the interaction of H_2 and CO with Fe_2O_3 based on hydrogen-based shaft furnace process, *Int. J. Hydrogen Energy*, 70(2024), p. 39.
[20] Y. Wang and Z.S. Li, A DFT-based microkinetic theory for Fe_2O_3 reduction by CO in chemical looping, *Proc. Combust. Inst.*, 39(2023), No. 4, p. 4447.
[21] Z.S. Li, J.Z. Cai, and L. Liu, A first-principles microkinetic rate equation theory for heterogeneous reactions: Application to reduction of Fe_2O_3 in chemical looping, *Ind. Eng. Chem. Res.*, 60(2021), No. 43, p. 15514.
[22] J. Liu, X.X. Li, L. Guo, *et al*., Reaction analysis and visualization of ReaxFF molecular dynamics simulations, *J. Mol. Graph. Model.*, 53(2014), p. 13.
[23] T.P. Senftle, S. Hong, M.M. Islam, *et al*., The ReaxFF reactive force-field: Development, applications and future directions, *npj Comput. Mater.*, 2(2016), art. No. 15011.
[24] K. Chenoweth, A.C. van Duin, and W.A. Goddard, ReaxFF reactive force field for molecular dynamics simulations of hydrocarbon oxidation, *J. Phys. Chem. A*, 112(2008), No. 5, p. 1040.
[25] J.E. Mueller, A.C.T. van Duin, and W.A. Goddard III, Application of the ReaxFF reactive force field to reactive dynamics of hydrocarbon chemisorption and decomposition, *J. Phys. Chem. C*, 114(2010), No. 12, p. 5675.
[26] S. Agrawalla and A.C.T. van Duin, Development and application of a ReaxFF reactive force field for hydrogen combustion, *J. Phys. Chem. A*, 115(2011), No. 6, p. 960.
[27] C.Y. Zou and A. van Duin, Investigation of complex iron surface catalytic chemistry using the ReaxFF reactive force field method, *JOM*, 64(2012), No. 12, p. 1426.
[28] Y.K. Shin, H. Kwak, A.V. Vasenkov, D. Sengupta, and A.C.T. van Duin, Development of a ReaxFF reactive force field for Fe/Cr/O/S and application to oxidation of butane over a pyrite-covered Cr_2O_3 catalyst, *ACS Catal.*, 5(2015), No. 12, p. 7226.
[29] V. Strezov, Iron ore reduction using sawdust: Experimental analysis and kinetic modelling, *Renew. Energy*, 31(2006), No. 12, p. 1892.
[30] L. Guo, H. Gao, J.T. Yu, Z.L. Zhang, and Z.C. Guo, Influence of hydrogen concentration on Fe_2O_3 particle reduction in fluidized beds under constant drag force, *Int. J. Miner. Metall. Mater.*, 22(2015), No. 1, p. 12.
[31] J.H. Zhang, S.Y. Li, and L.W. Wang, Kinetics analysis of direct reduction of iron ore by hydrogen in fluidized bed based on response surface methodology, *Int. J. Hydrogen Energy*, 49(2024), p. 1318.
[32] X.D. Mao, P. Garg, X.J. Hu, *et al*., Kinetic analysis of iron ore powder reaction with hydrogen—Carbon monoxide, *Int. J. Miner. Metall. Mater.*, 29(2022), No. 10, p. 1882.
[33] J.L. Sun, B.Y. Huang, J.Q. He, E.C. Meng, and Q.H. Chang, Achieving oxidation protection effect for strips hot rolling via Al_2O_3 nanofluid lubrication, *Int. J. Miner. Metall. Mater.*, 30(2023), No. 5, p. 908.
[34] S. Yang, J.Y. Wu, H.W. Jing, *et al*., Molecular mechanism of fly ash affecting the performance of cemented backfill material, *Int. J. Miner. Metall. Mater.*, 30(2023), No. 8, p. 1560.
[35] A. Shams and F. Moazeni, Modeling and simulation of the MIDREX shaft furnace: Reduction, transition and cooling zones, *JOM*, 67(2015), No. 11, p. 2681.
[36] X. Jiang, L. Wang, and F.M. Shen, Shaft furnace direct reduction technology—Midrex and Energiron, *Adv. Mater. Res.*, 805-806(2013), p. 654.
[37] Y.Z. Ji, Z.Y. Chi, S.F. Yuan, *et al*., Development and application of hydrogen-based direct reduction iron process, *Processes*, 12(2024), No. 9, art. No. 1829.
[38] P. Ziesche, S. Kurth, and J.P. Perdew, Density functionals from LDA to GGA, *Comput. Mater. Sci.*, 11(1998), No. 2, p. 122.
[39] P. Haas, F. Tran, P. Blaha, K. Schwarz, and R. Laskowski, Insight into the performance of GGA functionals for solid-state calculations, *Phys. Rev. B*, 80(2009), No. 19, art. No. 195109.
[40] W. Humphrey, A. Dalke, and K. Schulten, VMD: Visual molecular dynamics, *J. Mol. Graph.*, 14(1996), No. 1, p. 33.
[41] A. Stukowski, Visualization and analysis of atomistic simulation data with OVITO–the Open Visualization Tool, *Model. Simul. Mater. Sci. Eng.*, 18(2010), No. 1, art. No. 015012.
[42] Z.C. Zhao, J. Tang, M.S. Chu, *et al*., Direct reduction swelling behavior of pellets in hydrogen-based shaft furnaces under typical atmospheres, *Int. J. Miner. Metall. Mater.*, 29(2022), No. 10, p. 1891.
[43] L.Y. Yi, Z.C. Huang, T. Jiang, L.N. Wang, and T. Qi, Swelling behavior of iron ore pellet reduced by H_2–CO mixtures, *Powder Technol.*, 269(2015), p. 290.

2023 Innovative Young Scientist

Zhengjian Liu, born in 1982, is a professor at the School of Metallurgical and Ecological Engineering in University of Science and Technology Beijing. He has participated in more than 100 key projects including the National Natural Science Foundation of China, the National Key R&D Program of China, cooperative projects with Shougang and other domestic enterprises, as well as international cooperation between China and Russia, Rep. of Korea, Germany, and Switzerland. He has published more than 90 SCI/EI papers as the first or corresponding author. He has won 6 first prizes at provincial and ministerial levels (the one ranked first), authorized more than 60 patents, including 1 foreign patent, published 5 monographs, including 1 English monograph, and participated in drafting and introducing 1 national standard. He was a member of the International Scientific Committee of the 10th International Congress on the Science and Technology of Ironmaking (ICSTI2025), the lead person of the Ironmaking Technology Section of the 9th Asian Iron and Steel Congress, and the chairman of the Ironmaking and Raw Materials Section of the 10th, 11th, and 12th China Society of Metals Youth Academic Annual Meeting. He serves as an editorial board member of *Metals*, *Sintering and Pelletizing*, and *Iron and Steel Research*.